Glassy states in adsorbing surfactant-microgel soft nanocomposites

Sarah Goujard, Jean-Marc Suau, Arnaud Chaub, Jean-Michel Guigner, Thomas Bizien, Michel Cloitre

Glassy states in adsorbing surfactant-microgel soft nanocomposites

Sarah Goujard [(1)], Jean-Marc Suau [(2)], Arnaud Chaub [(1)], Jean-Michel Guigner [(3)], Thomas Bizien [(4)], Michel Cloitre [(1)]*

[1] Molecular, Macromolecular Chemistry and Materials, ESPCI Paris, CNRS, PSL University, 10 rue Vauquelin, 75005 Paris, France

[2] Coatex SAS, 35 Rue Ampère, 69730 Genay, France

[3] Sorbonne Université, CNRS, UMR 7590 Institut de Minéralogie, de Physique des Matériaux et de Cosmochimie (IMPMC)-IRD-MNHN, 75005 Paris, France

[4] Synchrotron SOLEIL, L'Orme des Merisiers, Saint-Aubin BP 48, Gif-sur-Yvette 91190, France

* michel.cloitre@espci.psl.eu; orcid: 0000-0002-0869-6730

Abstract

Mixtures of polymer-colloid hybrids such as star polymers and microgels with non-adsorbing polymeric additives have received a lot of attention. In these materials, the interplay between entropic forces and softness is responsible for a wealth of phenomena. By contrast, binary mixtures where one component can adsorb onto the other one have been far less studied. Yet real formulations in applications often contain low molecular weight additives that can adsorb onto soft colloids. Here we study the microstructure and rheology of soft nanocomposites made of surfactants and microgels using linear and nonlinear rheology, SAXS experiments, and cryo-TEM techniques. The results are used to build a dynamical state diagram encompassing various liquid, glassy, jammed, metastable, and reentrant liquid states, which results from a subtle interplay between enthalpic, entropic, and kinetic effects. We rationalize the rheological properties of the nanocomposites in each domain of the state diagram, thus providing exquisite solutions for designing new rheology modifiers at will.

1. Introduction

Modern formulations encountered in personal care products [1,2], foodstuff [3], paint and coatings [4] are complex mixtures containing multiple components such as colloids, polymers, surfactants, or liquid droplets. The addition of polymers, proteins, or nanoparticles - the so-called small components of the formulation -, to colloidal suspensions - the large components- can be responsible for a variety of phenomena depending on the nature of the intermolecular interactions at work. For instance, the adsorption of polymers, proteins, or nanoparticles onto colloids can lead to steric stabilization [5,6] or bridging flocculation [6], depending on the degree of coverage and the existence of possible multiple attractions mediated by the small component. If the small component is not adsorbed, osmotic pressure effects are responsible for attractive depletion interactions which are at the origin of new and important phenomena [7]. To meet the severe requirements imposed by technological applications in terms of stability and flow properties, and to be able to design new products in a rational way, it is essential to control the interactions and the microstructure of mixtures at multiple length scales, over a wide range of concentration, from a soft condensed matter physics perspective.

This topic has received considerable attention over the last two decades essentially for the case of mixtures involving non-adsorbing components [8,9]. Mixtures of hard sphere colloids and linear polymer have been extensively studied both experimentally and theoretically. They exhibit a rich morphology diagram primarily controlled by depletion forces, which encompasses aggregates, gels, crystals, repulsive and attractive glasses [10-13]. Of particular interest is the high volume fraction regime where addition of free polymer to a repulsive glass melts the glass and, at higher polymer content, provokes freezing into a re-entrant attractive glass [11-16]. The dynamics and the rheology of attractive glasses result from the interplay between cage effect where particles are topologically trapped in the environment formed by their neighbours and bond formation originating from attractive forces [17].

Glass melting and reentrance also occur when polymer is added to colloids interacting through soft potentials such as microgels and star polymers [18-20]. Soft colloids have the capacity to adjust their shape and volume to the osmotic pressure of the linear chains by deforming and deswelling. The interplay between depletion and particle shrinkage has two important consequences that make soft colloids inherently different from hard spheres. First, the liquid-like domain between repulsive and attractive glasses at intermediate concentrations of linear polymers has a greater extent than in soft colloids [21,22]. Secondly, for mixtures of ultrasoft stars and linear polymer chains the reentrant solid at high polymer concentrations is a soft gel and not an attractive glass [21-25]. This paradigm has been extended to binary mixtures of colloids with variable softness, offering many different combinations of interactions. In soft star-hard particles mixtures, a wealth of possible physical states - liquid phase, repulsive glasses, double glasses, arrested phase separation - has been discovered and analysed theoretically [26-29].

Soft colloids are intrinsically permeable in addition of being deformable. As a consequence, additives can adsorb inside soft colloids under some conditions. For instance, linear chains have the capacity to penetrate star polymers if their molar mass is smaller than the molecular mass of the star arms [30]. Similarly, loosely crosslinked microgels can be partially swollen by linear chains, whereas the chains are excluded when the crosslinked density is high [22-34]. Penetration of soft colloids by free polymer chains has new and important consequences. First, attractive depletion forces are reduced, which is beneficial to dispersing soft colloids inside polymer matrixes [22,31,33]. Secondly, the enthalpic interactions associated to the adsorption of the polymer change the solvent quality, which provokes the swelling or shrinkage of the colloids and affects the kinetic arrest of the mixtures [30,34]. Furthermore, it has been reported that, besides polymer chains, a number of small moieties such as nanoparticles [35], proteins [36], surfactants [37-41], and biological molecules [42] can be

adsorbed inside microgels also causing their swelling. The phase behaviour and rheology of these materials at high concentration pose new and interesting questions, which have remained unexplored. A great challenge is to control and model the state diagram and the rheological properties of mixtures with adsorbing components in terms of enthalpic and entropic interactions between polymeric networks and small guest molecules.

Here we address this question for soft nanocomposites obtained by mixing stimuli-responsive polyelectrolyte microgels with anionic surfactants. The adsorption of the surfactants inside the microgels is driven by the hydrophobic interactions between the polymeric network of the microgels and the surfactants tails leading to mixed polymer-surfactant micelles. A combination of linear and non-linear rheology measurements with Small Angle X-ray Scattering and cryo-transmission electron microcopy experiments allow us to construct a rich state diagram encompassing liquid, glassy, jammed, and reentrant liquid states. At low polymer concentration, the nanocomposites are viscous liquids at any surfactant content but, at large enough concentration, the particles jam and form glasses with viscoplastic properties. When the surfactant concentration is high enough, the glasses melt and a reentrant solid-liquid transition takes place. This transition is associated with distortions of the local structure due to microphase separation phenomena induced by depletion attractive forces. We rationalize the rheological properties of the nanocomposites over the entire state diagram, which provides exquisite solutions to design rheology modifiers at will.

2. Experiments

2.1 Microgel synthesis and characterization

The studied microgels are copolymers of ethyl acrylate (0.624 mol.mol^{-1}), methacrylic acid (0.372 mol.mol^{-1}) and the difunctional crosslinker diallyl phthalate (0.004 mol.mol^{-1}). They are synthesized at low pH by radical emulsion polymerization using a semi-batch protocol in starved-feed conditions during which initiators and reactants are continually added. The synthesis conditions and, in particular, the temperature and the feeding rates are precisely

adjusted to ensure a constant conversion rate, which is known to avoid inhomogeneity of composition and microstructure [43,44]. At the end of the synthesis, we obtain a stock suspension of spherical colloidal particles. The solid content of the suspension is accurately measured by thermogravimetry. The radius of gyration (R_g) and the hydrodynamic radius (R_h) of the particles are determined by Small Angle X-ray Scattering and Dynamic Light Scattering as described in Section 2.4 below: $R_g = 27$ nm and $R_h = 35$ nm leading to a ratio $R_g / R_h \simeq 0.75$ which is close to the characteristic value expected for hard-spheres (0.775). The size distribution is weakly polydisperse with a mean-square deviation less than 0.1. Since the microgels are made of a hydrophobic polymer, they are insoluble in water at acidic and even neutral pH. They need to be activated by some stimuli to express their functional properties. A conventional method consists in adding a base that ionizes the methacrylic acid units and increases the pH to the range 8.5-9. The osmotic pressure of the counterions provokes the expansion of the crosslinked polyelectrolyte network resulting in a significant swelling of the particles [45,46]. Upon complete ionization, the hydrodynamic radius of the microgels used in this study is $R_h = 165$ nm which represents an increase of the effective volume by more than a factor 100. Although this strategy is very efficient, it cannot be used in applications such as cosmetic, galenic, and personal care products which must respect the slightly acidic pH of the skin.

2.2 Preparation of microgel-surfactant nanocomposites

In this work, microgels are activated by adding surfactant molecules that adsorb onto the polyelectrolyte network and provoke the swelling of the microgels. We use sodium dodecyl sulfate (SDS), $CH_3(CH_2)_{11}OSO_3Na$, commercially available from Sigma Aldrich (ACS Reagent, purity >99%). Using conductimetry and interfacial tension measurements, we determined that SDS has a critical micellar concentration in pure water of about 2.3 $mg.g^{-1}$ [47]. Nanocomposites are prepared by mixing equal volume of aqueous solutions containing the requested amount of surfactant and microgels. After mixing, the suspensions are gently stirred for 24 hours using a VWR microplate shaker, to ensure good homogeneity, and kept at rest for at least another 24 hours before use. At high microgel concentration, nanocomposites exhibit

yielding properties and may entrap air bubbles which are removed before use by gentle centrifugation. In the following *C* and *S* denote the concentrations of microgels and surfactant expressed in mass fraction ($mg.g^{-1}$).

2.3 Rheological measurements

Rheological measurements are performed using a stress-controlled rheometer (Anton Paar MCR 502) equipped with a cone and plate geometry (50 mm in diameter and 2° angle) and optionally with a double-gap Couette geometry (ref DG27) for the less viscous suspensions. The shearing surfaces are roughened by sandblasting to prevent slip. After loading, the surfactant-microgel nanocomposites are isolated from the ambient atmosphere by a solvent trap to minimize water evaporation. The interior atmosphere of the trap is saturated using a small volume of distilled water. The bottom plate is connected to a Peltier system that controls the temperature at 20.0±0.1 °C.

Small amplitude oscillatory shear (SAOS) experiments are used to probe the linear viscoelastic properties of the nanocomposites and establish their rheological state diagram. The storage modulus *G'* and loss modulus *G''* are measured by applying an oscillatory strain of small amplitude $\gamma_0 = 0.01$, the angular frequency ω varying between 10^{-3} and 10^{2} $rad.s^{-1}$. The viscoelastic spectra of the solid-like composites have the characteristic shape exhibited by many soft solids, i.e. a nearly constant storage modulus and a much lower loss modulus with a shallow minimum around a frequency ω_m. The value of the storage modulus at ω_m is taken as the low-frequency plateau modulus G_0 of the suspensions.

In steady shear experiments, the stress σ or equivalently the viscosity η are measured as a function of the applied shear rate $\dot{\gamma}$. At each applied shear rate between 10^{3} and 10^{-4} s^{-1}, the stress and viscosity are recorded after they reach steady state values. Steady shear experiments are complemented in the low rate domain by creep measurements which consists in applying a constant stress value close to the yield stress and recording the strain evolution versus time, $\gamma(t)$. Steady flow is signalled by a linear increase of $\gamma(t)$ with time resulting in a constant shear rate $\dot{\gamma}$. Liquid nanocomposites possess the characteristic behaviour of colloidal suspensions: the viscosity $\eta(\dot{\gamma})$ exhibits a constant Newtonian viscosity η_0 at low shear rates,

followed by shear thinning as the shear rate is increased. The experimental variations are well modelled by the Carreau–Yasuda equation [48]:

$$\sigma(\dot{\gamma}) = \dot{\gamma}\left\{\eta_\infty + \frac{\eta_0 - \eta_\infty}{\left[1+\left(\dot{\gamma}\tau_0\right)^\alpha\right]^\beta}\right\}, \quad (1)$$

where η_0 and η_∞ are the low- and high-shear viscosities, τ_0 is the longest relaxation time which characterizes the onset of shear-thinning, α and β are two exponents (with $\beta \cong 1$). Solid nanocomposites are yield stress materials with the stress being well described by the Herschel-Bulkley equation:

$$\sigma(\dot{\gamma}) = \sigma_y + k\dot{\gamma}^n \ , \quad (2)$$

where *k* is the consistency parameter and *n* the shear thinning exponent.

2.4 Scattering methods

Fairly dilute microgel-surfactant nanocomposites are optically transparent, allowing the use of standard Dynamic Light Scattering (DLS) to measure the evolution of the hydrodynamic radius upon surfactant addition. The setup is a CGS3 Compact Goniometer System from ALV, equipped with a Helium–Neon laser emitting at 632.8 nm and an ALV-LSE 5004 digital correlator. The suspensions to be studied are contained into cylindrical borosilicate test tubes (diameter: 10 mm) commercially available from VWR. The tubes are inserted in a temperature-regulated cuvette filled with toluene which is placed on a motor-driven precision goniometer. The scattering wavevectors q are varied between 6.8×10^{-3} nm^{-1} and 2.6×10^{-2} nm^{-1}. Time-averaged intensity correlation functions are recorded for about 300 s and analysed using the classical cumulant method that provides the decay rate $\Gamma = q^2 D$, D being the diffusion coefficient. In the limit of low volume fractions, we can use the Stokes-Einstein relationship to deduce the hydrodynamic radii R_h of the particles:

$$D = \frac{k_B T}{6\pi\eta_s R_h} \quad (3)$$

η_s = 0.89 mPa.s is the solvent viscosity which is taken equal to the viscosity of water at 20°C.

Small-angle X-rays scattering (SAXS) experiments are conducted at the Synchrotron Soleil facility (Saint-Aubin, France) on the small angle scattering beamline SWING. The X-ray wavelength is $\lambda = 1.03$ Å. Two sample to detector distances are used in combination to explore a wide *q*-range, ranging from 1.1×10^{-3} Å^{-1} to 0.66 Å^{-1}. 2D scattering patterns are collected by a EIGERX 4M detector, normalized by the transmitted intensity, and azimuthally averaged to get 1D spectra. The nanocomposites are loaded in sealed quartz capillaries (diameter: 1.5 mm) provided by WJM Glass (Reference Q-15-001-80). For each studied sample, three capillaries are filled and for each capillary five different locations are explored. At each location 5 spectra are recorded with exposure times of 750 ms separated by dead times of 5 s. Background spectra from capillaries filled with pure water are recorded in a similar way. Data processing involves a series of operations, i.e. background subtraction, averaging, merging of spectra over different *q*-ranges, which are performed using the software Foxtrot developed at the beamline [49]. The spectra presented in this paper result from averages over the different measuring points in the three capillaries.

2.5 Cryo-TEM experiments

Cryo-transmission electron microscopy (cryo-TEM) observations are conducted on a JEOL JEM 2100 microscope (JEOL, Japan) equipped with a Minimum Dose System which reduces irradiation during imaging. The camera is an Ultrascan 1000 which has a 2k x 2k pixel CCD (Gatan, USA). The samples are prepared by depositing a drop of nanocomposite solution on a grid previously treated to render its surface hydrophilic (Quantifoil from Micro Tools GmbH, Germany). The excess of solution is carefully sucked out with a filter paper. The grid is plunged in liquid ethane leading to the instantaneous vitrification of the material. The grid is then mounted on a Gatan 626 cryo-holder cooled with liquid nitrogen and transferred into the microscope.

3. Results and discussion

3.1 Surfactant adsorption and microgel swelling

As surfactant is added to the microgels, the turbidity of the solutions significantly decreases indicating that the volume of the microgel particles increases. Swelling is monitored by

measuring the hydrodynamic radius of the microgels in dilute solutions using DLS, as a function of the quantity of added surfactant. A typical titration curve is shown in figure 1. The microgel start swelling at a finite surfactant concentration called the critical aggregation concentration (CAC ≅ 1 $mg.g^{-1}$), which marks the onset of formation of surfactant-polymer complexes. The CAC is found almost independent of the microgel concentration as found in surfactant-linear polymer mixtures [50]. Above CAC, the hydrodynamic radius rapidly increases with the surfactant content and reaches a plateau. In figure 1, the hydrodynamic radius at maximum swelling is 103 nm, yielding a volume swelling ratio $Q \cong 26$. We associate the plateauing of the hydrodynamic radius to the saturation of the microgels when they reach their maximum adsorption capacity. Using fluorescence spectroscopy techniques, we have shown that, above saturation, the excess surfactant molecules associate into free micelles that coexist with the swollen microgels [47]. The molecular mechanisms at the origin of adsorption and polymer-surfactant complex formation are beyond the scope of this paper and will be studied in a separate paper.

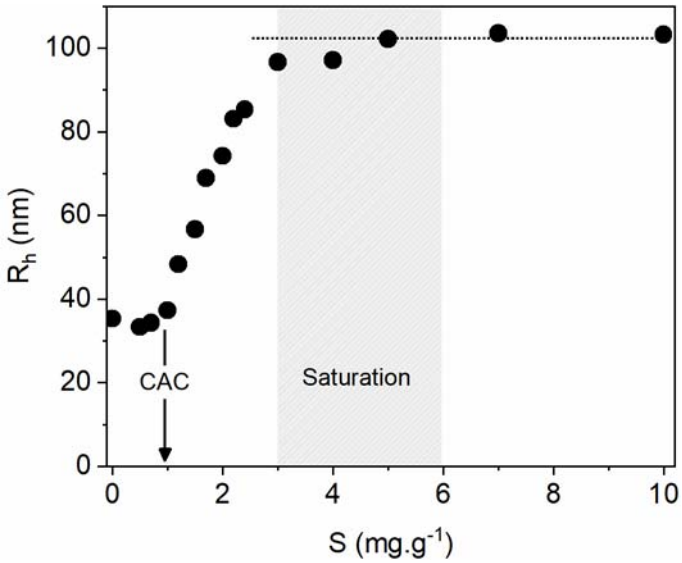

Figure 1. Evolution of the hydrodynamic radius of microgels with the quantity of SDS added (C = 0.5 $mg.g^{-1}$). The arrow points to the critical aggregation concentration (CAC) and the horizontal dashed line is a guide to the eye. The range of concentration where saturation occurs and swelling stops is highlighted in grey.

3.2 Rheological fingerprinting of microgel-surfactant nanocomposites

3.2.1 Linear viscoelastic properties. In this section we use SAOS experiments to probe the viscoelastic properties of the nanocomposites. At low polymer concentrations, when C is smaller than $C_m \cong 18$ mg.g^{-1}, the viscoelastic spectra of the nanocomposites systematically exhibit a terminal regime which extends over almost the entire frequency range indicating that they are viscous suspensions [47]. At higher polymer concentrations, when C is larger than C_m, much richer behaviour is found when the surfactant concentration is increased. Representative viscoelastic spectra are presented in figure 2, where the storage and loss moduli G' and G'' are plotted for $C = 25$ mg.g^{-1} and increasing surfactant concentrations. Similar results are obtained for the other microgel concentrations [47]. Here we limit our study to a range of surfactant concentrations ($S \leq 120$ mg.g^{-1}) where sodium dodecyl sulfate micelles are not expected to experience morphological transitions [51], which will be further confirmed by the SAXS experiments presented in section 3.3.3.

At low surfactant concentration, typically for $S = 20$ mg.g^{-1} (figure 2(a)), the viscoelastic spectra show a terminal regime where $G'(\omega) \propto \omega^2$ and $G''(\omega) \propto \omega$ over two decades of frequency (from 10^{-2} to 2×10^{0} rad.s^{-1}), which is the signature of liquid behaviour. At $C = 21$ mg.g^{-1} (figure 2(b)), the nanocomposite is a viscoelastic solid with a weak storage modulus plateau that is larger than the loss modulus. The onset of terminal behaviour is detected at the lowest angular frequency. This is the characteristic viscoelastic behaviour of entropic glasses [46]. At intermediate SDS concentration, i.e. for $S = 30$ mg.g^{-1} (figure 2(c)), the storage modulus G' follows a plateau which is larger than the loss modulus G'' over the entire frequency window. G" is about an order of magnitude smaller than G' with a shallow minimum at intermediate frequencies. Terminal relaxation is not accessible. At this concentration, the nanocomposite is a jammed glass with repulsive interactions [46, 52]. As the surfactant concentration is further increased, i.e. at $S = 80$ mg.g^{-1} (figure 2(d)), the storage modulus still exhibits a plateau modulus over the entire range of frequency explored but it is smaller than in figure 2(c). At $S = 100$ mg.g^{-1} (figure 2(e)) the plateau modulus is limited to the range of frequency above $\omega \cong 0.1$ rad.s^{-1}; at lower frequencies, terminal regime is recovered indicating that the nanocomposites have returned to the liquid state. The same process continues and at

still larger surfactant concentrations, i.e. for $S = 120$ mg.g^{-1} (figure 2(f)), both moduli are smaller, terminal relaxation is observed over two decades of frequencies making the viscoelastic properties similar to those observed at low surfactant concentrations. In conclusion, SAOS experiments appear to be a power tool to fingerprint the mechanical behaviour of soft

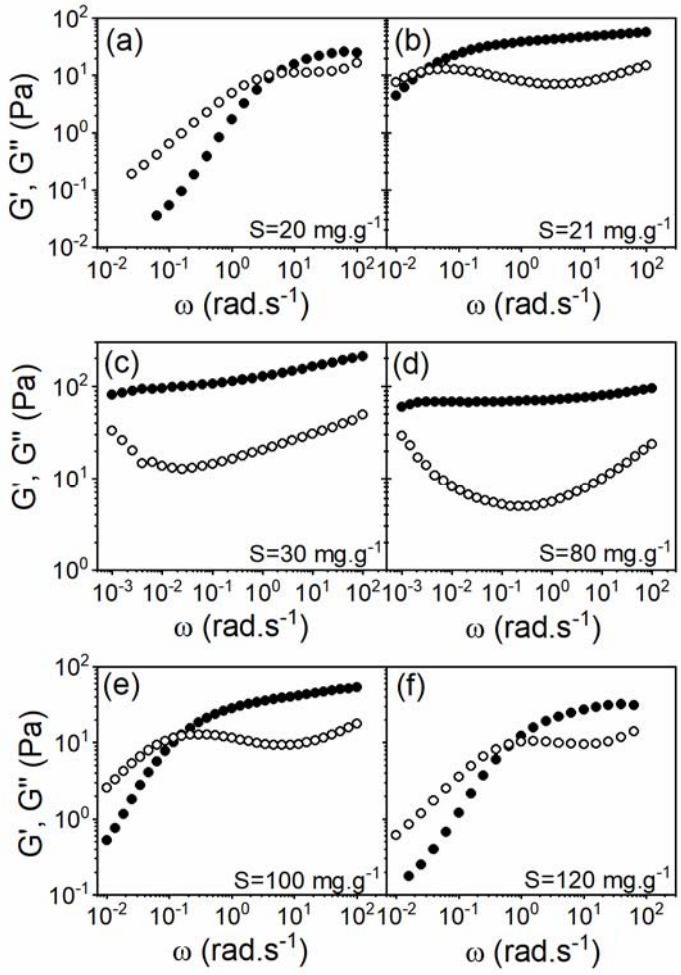

Figure 2. Frequency-dependent storage (●) and loss (○) moduli of microgel-surfactant nanocomposites for increasing surfactant concentration (from left to right and top to bottom) at constant microgel concentration, $C = 25$ mg.g^{-1}.

nanocomposites. Upon surfactant addition, the microgels swell causing an increase of the volume fraction and several dynamical states are encountered: viscous liquids, entropic glasses, jammed phases, and reentrant liquid phases.

3.2.2 Steady flow rheology. Steady-shear rheology is used to characterize the flow behaviour of composites with the same microgel concentration as in the previous section ($C = 25$ mg.g^{-1})

and SDS concentrations increasing from 5 to 120 mg.g^{-1}. Figure 3 shows the evolution of the shear stress σ at steady state as a function of the applied shear rate $\dot{\gamma}$. For clarity, the figure is split

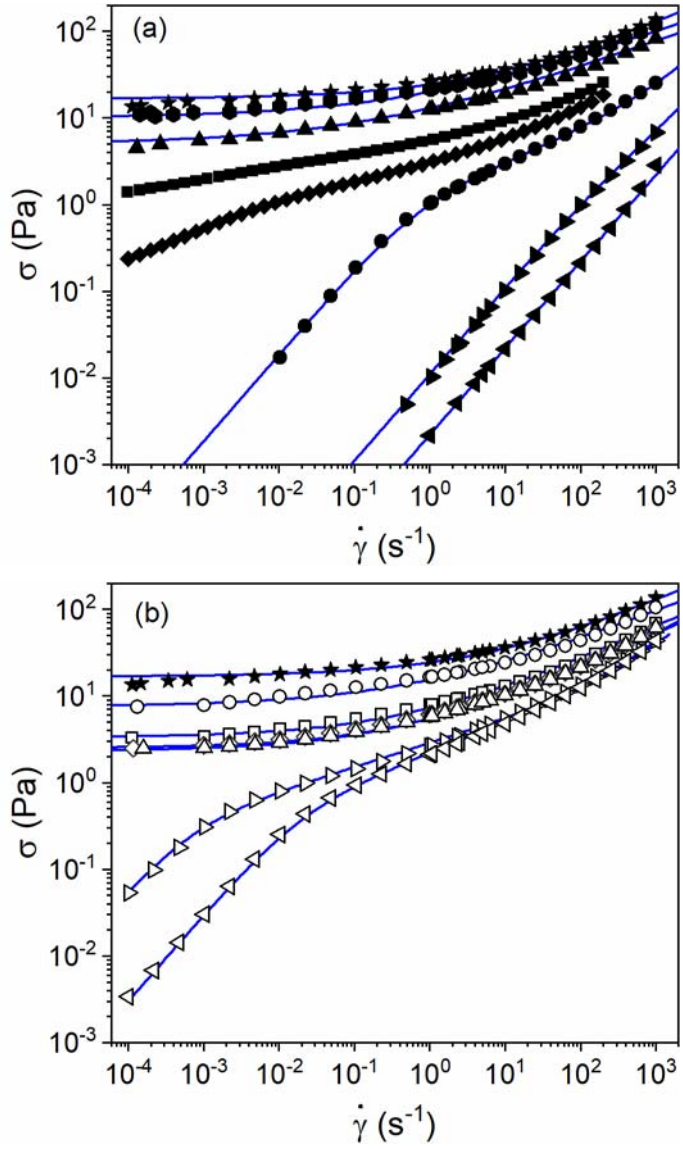

Figure 3. Stress-shear rate relationships for microgel-surfactant nanocomposites with constant microgel concentration (C = 25 mg.g^{-1}) and increasing surfactant concentrations. (a): S = 5 (◀), 10 (▶), 20 (●), 21 (◆), 22 (■), 30 (▲), 35 (⬢), and 40 (★) mg.g^{-1}; in this range of concentration, the stress increases with the surfactant content. (b): S = 40 (★), 50 (○), 60 (□), 70 (◇), 80 (△), 100 (▷), and 120 (◁) mg.g^{-1}; the stress decreases with the surfactant concentration. The lines are the best fits of the experimental data to the Carreau-Yasuda (for viscoelastic liquids) and Herschel-Bulkley (for yield stress fluids) equations.

into two panels. In figure 3(a) ($C \leq 40$ mg.g^{-1}) the stress increases with the surfactant concentration whereas in figure 3(b) ($C \geq 40$ mg.g^{-1}) it decreases. In figure 3(a), when S = 5 and 10 mg.g^{-1}, the stress is proportional to the shear rate over the entire range of shear rate,

indicating Newtonian behaviour. For S = 20 mg.g^{-1}, Newtonian behaviour is still observed at low shear rates but the suspension becomes strongly shear-thinning at high shear rates. The flow curve is well fitted to the Carreau-Yasuda equation allowing to determine the low-shear viscosity. The rheological properties change very rapidly and for S = 21 and 22 mg.g^{-1}, Newtonian behaviour is no longer observed. These nanocomposites are entropic glasses as discussed in the previous section (see figure 2(b)). At higher SDS concentration, we enter the jammed glass regime (see figure 2(c)) and the flow curves exhibit the characteristic shape expected for yield-stress fluids, i.e. a stress plateau at low shear rates followed by an increase of the stress at higher shear rates. They are well fitted to the Herschel-Bulkley equation allowing to determine the yield stress σ_y . The yield stress increases with the SDS concentration, goes through a maximum for S = 40 mg.g^{-1}, then decreases as the elasticity diminishes (figure 2(e)) and finally vanishes. For S = 100 and 120 mg.g^{-1}, the nanocomposites return to the liquid state in agreement with figures 2(e) and 2(f).

3.2.3 Dynamical arrest of liquid composites at the glass transition. The low-shear viscosity η_0 of the liquid nanocomposites is determined by fitting the flow curves $\sigma(\dot{\gamma})$ to the Carreau-Yasuda equation. The variations of η_0 with the surfactant concentration are plotted in figure 4. At very small surfactant concentration, where the microgels are collapsed or weakly swollen (figure 1), the viscosity is close to that of the solvent. When more surfactant is added, the microgels swell and the viscosity rapidly increases. In the range of surfactant concentration investigated here, the contribution of the collapsed microgels to the viscosity is at most 10% of the solvent viscosity. For $S = 5$ mg.g^{-1}, the viscosity is about 2.5 times larger than the solvent viscosity. At higher surfactant concentrations, two situations can be distinguished. At low microgel concentration ($C \leq 18$ mg.g^{-1}), η_0 increases with the SDS concentration, reaches a maximum, and then decreases to a plateau value. At large microgel concentration (C >18 mg.g^{-1}), η_0 increases until it diverges. At this point, the composites are weak solids, in agreement with the viscoelasticity data discussed in the previous section. If the surfactant concentration is further increased, a reentrant solid-liquid transition eventually takes place and it is again possible to measure a low-shear viscosity (see also figures 2 and 3). The reentrant transition

occurs at a surfactant concentration that rapidly increases with the microgel concentration, so that the composites remain solid-like for $C \geq 30$ mg.g^{-1}.

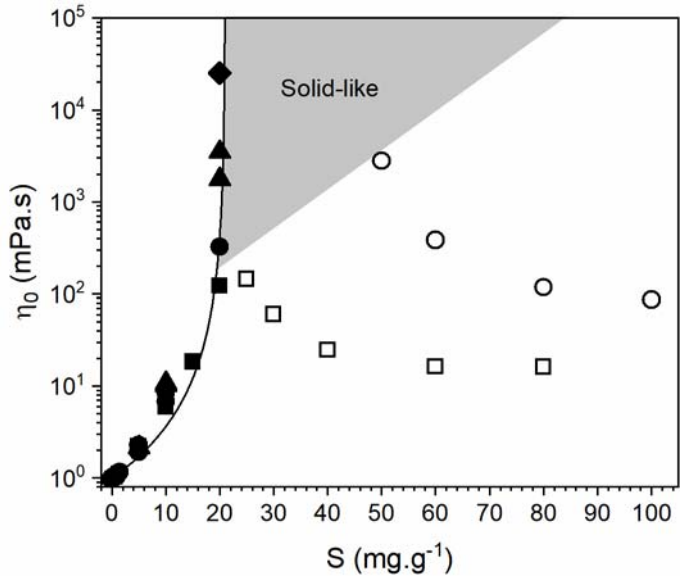

Figure 4. Variations of the low-shear viscosity of liquid nanocomposites as a function of the surfactant concentration. Each symbol refers to a microgel concentration: C = 15 (■, □), 20 (●, ○), 25 (▼), 30 (▲), 40 (◆) mg.g^{-1}. For C = 15 and 20 mg.g^{-1}, the viscosity first increases and diverges (full symbols) before decreasing (open symbols). The continuous line (equation 4) expresses the divergence of the viscosity at the surfactant concentration S_G.

In the following, we neglect the low surfactant concentration domain where the microgels are collapsed and we focus on the regime where the viscosity is controlled by the swelling of the microgels. Figure 4 shows that the values of the viscosity measured for different microgel concentrations collapse onto a master curve indicating that the low-shear viscosity mainly depends on the surfactant concentration. The master curve is reasonably well described by the equation:

$$\eta_0 = \eta_s \left(1 - \frac{S}{S_G}\right)^{-2}, \qquad (4)$$

where η_s is the solvent viscosity and $S_G = 21.0 \pm 0.5$ mg.g^{-1}. Thus the solidification of the nanocomposites at large enough microgel content is associated to a divergence of the low-shear viscosity. The divergence of the low-viscosity of hard sphere and soft microgel suspensions is a well-established phenomenon that has been widely discussed in the literature [45,46,53-57].

In general, the variations of the viscosity measured in experiments or computed numerically are expressed in terms of the particle volume fraction ϕ using an expression similar to equation 4 where the surfactant concentration is replaced by the volume fraction [53,54]. This suggests that the volume fraction of the swollen microgels and the surfactant concentration are simply proportional: $\phi = kS$, where k is a dimensionless coefficient. If we assume that the divergence of the viscosity corresponds to the dynamical arrest of the nanocomposites at the glass transition ($\phi_G = 0.58$), as found in hard sphere [57] and soft microgel [46] suspensions, the coefficient k is of the order of 0.027 g.mg^{-1}. This provides a method to estimate the volume fraction of the swollen microgels as a function of the surfactant content.

3.2.4 The jamming transition. Figure 5(a) depicts the variations of the plateau modulus of the nanocomposites (G_0) in the solid-like regime, as a function of the surfactant concentration for different microgel concentrations. For each microgel concentration, the elastic modulus first increases with the surfactant concentration until it reaches a maximum value for a surfactant concentration S_m, above which it decreases (see figure 2). At the lowest microgel concentrations investigated, i.e. $C = 20$ and 25 mg.g^{-1}, the elastic modulus vanishes at the solid-liquid re-entrant transition as shown in Section 3.2.1. Below the maximum ($S \leq S_m$), the values of the plateau modulus measured for different microgel concentrations collapse onto a master curve indicating that the elastic modulus of the nanocomposites is controlled by the surfactant concentration. The master curve is reasonably well described by the equation:

$$G_0 = \tilde{G}_0 \left(S - S_J \right), \tag{5}$$

where $\tilde{G}_0 = 32$ Pa.mg^{-1}.g and $S_J = 24 \pm 1$ mg.g^{-1}. The linear increase of the plateau modulus is a characteristic feature of jammed particulate dispersions [46,58,59]. In this regime, the nanocomposites can be described as disordered packings of athermal frictionless microgels interacting through elastic contact forces which are responsible for the elastic properties. The modulus increases with the concentration because both the number of contacts per particle and the compression of particles increase [59]. The concentration S_J defined from Eq. 5 is larger than the concentration S_G that marks the divergence of the viscosity in Eq. 4, confirming that S_J and S_G represent different transitions. S_G is the surfactant concentration for which the

microgel-surfactant suspensions become arrested entropic glasses whereas S_J characterizes the jamming transition. Similar observations have been made in similar polyelectrolyte microgels which are activated by charge ionization [46].

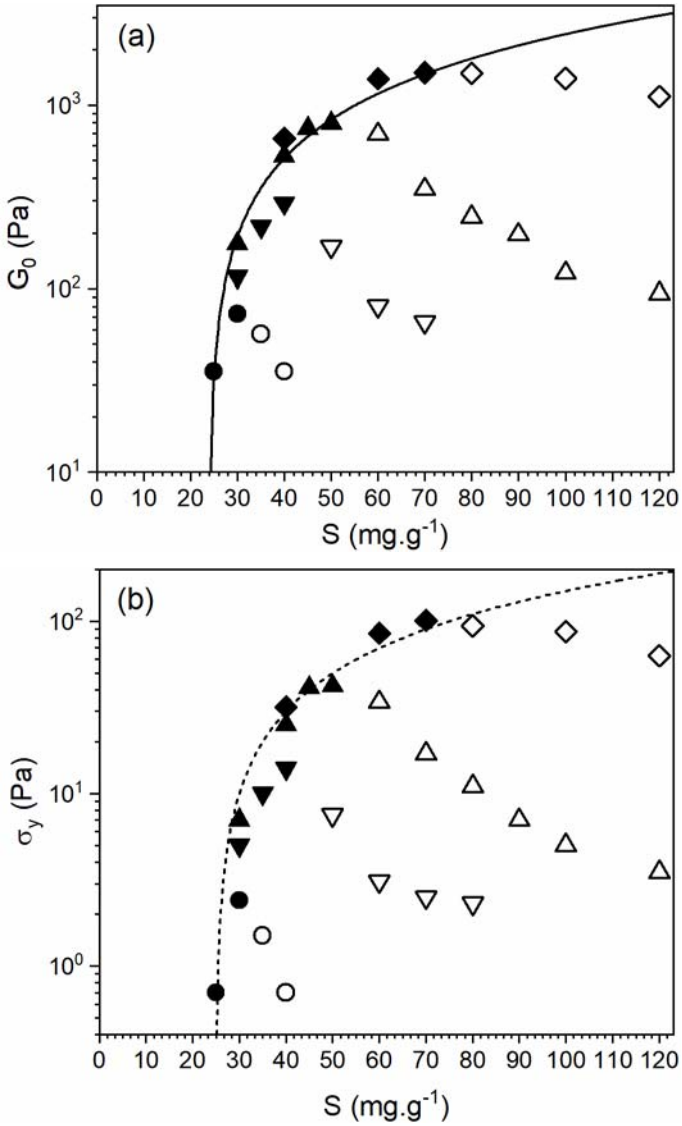

Figure 5. Variations of the low-frequency plateau modulus (a) and yield stress (b) of solid nanocomposites as a function of the surfactant concentration. The low-frequency modulus and the yield stress increase up to a surfactant concentration S_m (full symbols) and then decrease (open symbols). Each symbol refers to a microgel concentration: C = 20 (●, ○), 25 (▼, ▽), 30 (▲, △), 40 (◆, ◇) mg.g^{-1}; S_m = 30, 40, 50, and 70 mg.g^{-1}, respectively. The continuous line in (a) (equation 5) shows that for $S \le S_m$ the modulus increases linearly with the distance to the concentration S_J at the jamming point. The equation of the dotted line in (b) is $\sigma_y = G_0 \gamma_y$ with $\gamma_y = 0.057$.

In figure 5(b) we plot the variations of the dynamic yield stress σ_y determined from the flow curves presented in figure 3, as a function of the surfactant concentration. Remarkably, we

observe that the dynamic yield stress can be mapped onto the plateau modulus values. For each microgel concentration, σ_y first increases linearly with the surfactant concentration, reaches a maximum value around a surfactant concentration S_m, and then decreases and eventually vanishes. For $S \leq S_m$, the dynamic yield stress essentially depends on the surfactant concentration and is proportional to the plateau modulus through the yield strain coefficient γ_y which is of the order of 0.06; similar yield strain values have been found for microgel suspensions activated by charge ionization [46].

In the jammed regime, particles are trapped in cages formed by their neighbours with whom they interact through elastic repulsive forces. The flow properties of jammed suspensions of soft particles have been shown to exhibit universal properties when expressed in terms of the non-dimensional shear rate $\dot{\gamma}\eta_s / G_0$ which arises from the competition between the cage relaxation time η_s / G_0 and the advection time $\dot{\gamma}^{-1}$ [60,61]. The relaxation time η_s / G_0 results from the interplay between the viscous forces and the elastic restoring forces and sets the duration of shear-induced rearrangements. In figure 6, these predictions are evaluated for the case of our microgel-surfactant composites above the jamming transition ($S \geq S_J$), by plotting the flow curves shown in figure 3 (C = 25 mg.g^{-1}) using the reduced shear stress σ / σ_y and the non-dimensional shear rate $\dot{\gamma}\eta_s / G_0$. This set of scaling variables successfully collapses the flow curves except at large surfactant concentration larger than S_m. The master curve is well fitted to the Herschel-Bulkley equation $\sigma / \sigma_y = 1 + 95\left(\eta_s \dot{\gamma} / G_0\right)^{0.45}$. This form, and in particular the value of the exponent, is in good agreement with that found in experiments for other soft jammed colloids like concentrated emulsions [62], polyelectrolyte microgel suspensions [60], and in simulations of soft particle glasses [61]. In conclusion, the results obtained in this section demonstrate that concentrated surfactant-microgel composites can be described as jammed materials at low surfactant concentrations. However, the deviation of the rescaled data at large concentrations suggest that new phenomena take over at large surfactant concentrations. This motivates the structural study that is presented in the next section.

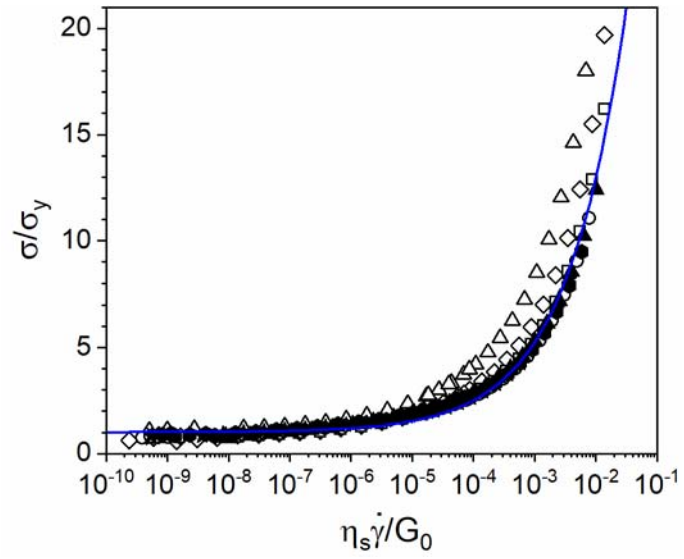

Figure 6. Flow curves in the jammed regime plotted using non dimensional variables. G_0 is the plateau modulus (values taken from figure 5) and $\eta_s = 0.89$ mPa.s is the viscosity of pure water. The microgel concentration is $C = 25$ mg.g^{-1}. Each symbol refers to a surfactant concentration: $S = 30$ (▲) , 35 (⬢), 40 (★), 50 (○), 60 (□), 70 (◇), 80 (△) mg.g^{-1}. The equation of the solid line is : $\sigma / \sigma_y = 1 + 95\left(\eta_s \dot{\gamma} / G_0\right)^{0.45}$.

3.3 Microstructure and interactions in microgel-surfactant nanocomposites

Figure 7 presents SAXS spectra and cryo-TEM micrographs of nanocomposites prepared with a microgel concentration C = 25 mg.g^{-1} and surfactant concentrations spanning the whole range of rheological states identified in section 3.2. A quantitative modelling of the full SAXS spectra would require to determine independently the form factors of the microgels and of the mixed surfactant-polymer micelles when the surfactant concentration varies, which is beyond the scope of this paper. In the following we consider separately the low/medium-q range ($q \leq 5\times10^{-2}$ Å^{-1})), which reflects the statistical distribution of the microgels in the composite, and the high-q range which results from the organization of the surfactant molecules adsorbed onto the polymeric network of the microgels.

3.3.1 Microstructure for $S \leq S_m$: liquid-like order and repulsive interactions. Figure 7(a) shows the scattering spectra measured upon adding surfactant up to $S_m = 40$ mg.g^{-1}. For $S = 0$ mg.g^{-1}, $I(q)$ compares well with the form factor of collapsed microgels which has been determined independently for low surfactant concentrations (data not shown). This is because the volume fraction is small so that the correlations between the microgels can be neglected.

The nanocomposites behave like dilute suspensions of hard spheres particles ($R_g = 27$ nm and $R_h = 35$ nm). The addition of surfactant dramatically changes the shape of the spectra since the volume fraction increases when the microgels swell and spatial correlations appear. All spectra exhibit a well-defined peak at q^*. Below q^*, $I(q)$ decreases to a constant plateau, which indicates that the interactions between the microgels are mainly repulsive. q^*, which is equal to 5×10^{-3} Å^{-1} when S = 5 mg.g^{-1}, increases with the surfactant concentration. For S = 10 mg.g^{-1} and 20 mg.g^{-1}, it is followed by secondary maxima of weaker amplitude at $2q^*$ and $3q^*$. These different peaks can be unambiguously attributed to the first, second, and third order peaks of the structure factor of liquid suspensions. This is nicely confirmed by the corresponding cryo-TEM micrograph, which shows individual microgels which are well separated one from another and arranged on a disordered lattice. The core of each microgel is surrounded by a corona at the periphery where the swelling is initiated.

For S = 30 mg.g^{-1}, the nanocomposites are jammed glasses. The higher order structural peaks have disappeared signalling a decrease in the interparticle correlations. On the micrograph, the microgels are uniformly arranged on a close-packed network, each microgel being in contact with many neighbours. For $S_m = 40\,\text{mg.g}^{-1}$ where the low-frequency modulus reaches its maximum value (see section 3.3.3), the spectra are not much changed suggesting that the microgels still form a jammed structure. The micrograph shows that the distribution of microgels is less uniform with some clustering which may indicate the possible existence of local association.

3.3.2 Microstructure for $S \geq S_m$: attractive interactions and arrested phase separation. In Figure 7(b), the different spectra are nearly superimposed above q^* indicating that the volume fraction no longer vary because the microgels have reached their maximum swelling. In other words, S_m represents the saturation concentration above which microgels no longer have the capacity to absorb surfactants molecules. The excess surfactant form free micelles confined in between the microgels. Interestingly, we can observe a small decrease and a broadening of the first structure factor peak and, at the largest surfactant concentrations investigated, an upturn of the intensity below q^*. In colloidal glasses, these observations are associated to a loss of spatial

correlations and the emergence of attractive interactions [11]. On the cryo-TEM micrograph relative to the reentrant liquid phase ($S = 120\,\mathrm{mg.g^{-1}}$), the particles are pushed together by the excess surfactant, resulting in large fluctuations in the microgel arrangement which form irregular patterns reminiscent of phase separation. These findings support the existence of attractive interactions and show that the reentrant transition is associated with phase separation.

3.3.3 Self-assembly and surfactant organization in composites. The variations of the intensity at high-q values are informative of the microstructures formed by the self-assembly of surfactants at small scale when they adsorb onto the polymer [50]. Surprisingly, the experimental data at high wavevectors qualitatively resemble the spectra measured for SDS micelles in pure water (inset of figure 7(b)), i.e. they have a deep minimum between two maxima, the amplitudes of which increase with the SDS concentration [51,63]. We note however that at small surfactant concentrations in figure 7(a), the minimum and the second maximum are significantly shifted to higher q values with respect to their positions for conventional SDS micelles. This shows that SDS form mixed surfactant-polymer micelles when they adsorb onto the polymeric network but that these mixed micelles are smaller than in the absence of polymer. In figure 7(b), above the saturation concentration S_m = 40 mg.g^{-1}, the minimum and second maximum are progressively shifted to lower wavevectors and, at the highest polymer concentration, they recover their values for SDS micelles in water. This confirms that the surfactant molecules in excess self-assemble outside the microgels into micelles which ultimately makes the dominant contribution to the scattered intensity. We attribute the attractive interactions above the saturation concentration to the existence of these micelles through at least two mechanisms: microgel bridging when micelles connect two of several neighbouring microgels, or depletion when the osmotic pressure of the micelles is large enough. The osmotic pressure exerted by the free micelles can also provoke a small deswelling of the microgels.

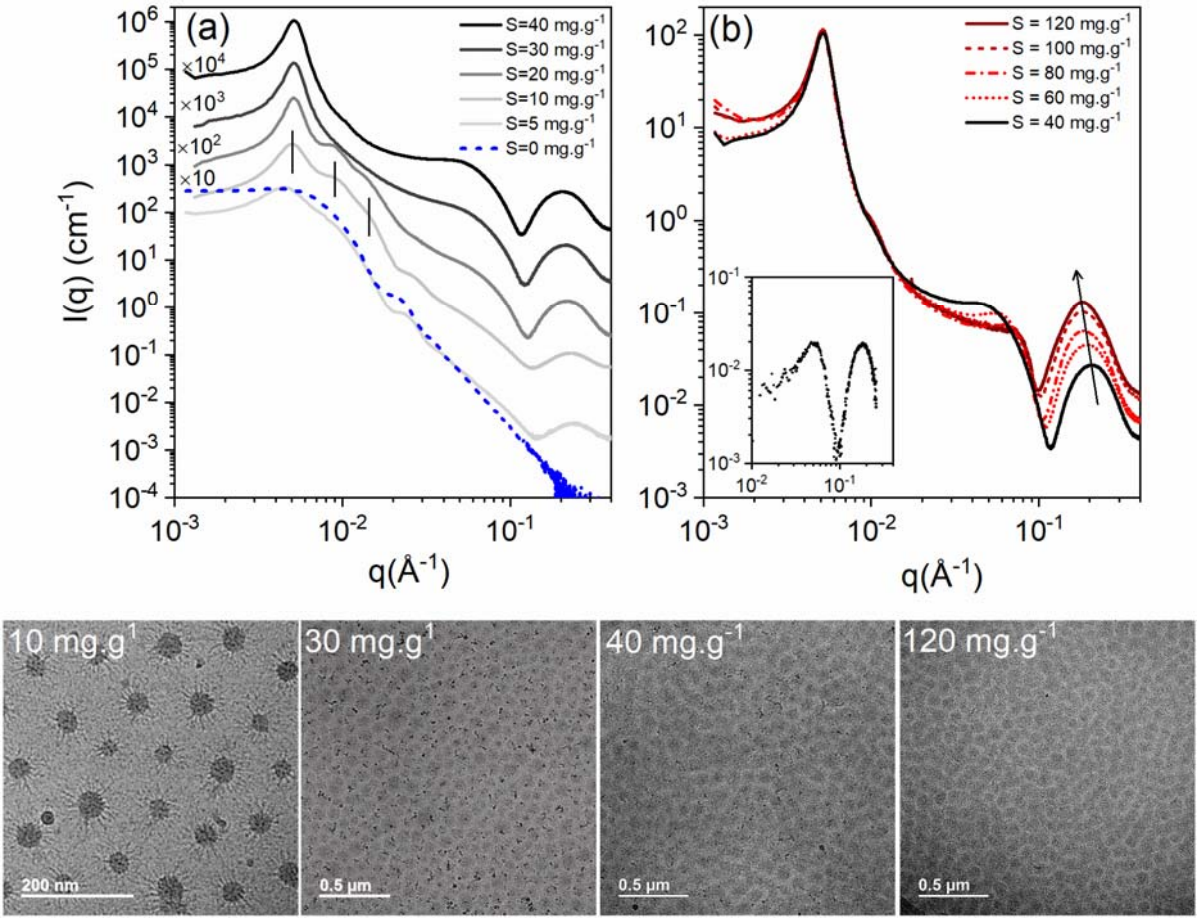

Figure 7. Microstructure of nanocomposites investigated by SAXS ((a) and (b)) and cryo-TEM micrographs (below); $C = 25$ mg.g^{-1}. In (a) the curves for $S = 10$, 20, 30, and 40 mg.g^{-1} are shifted vertically by a factor 10, 10^2, 10^3, and 10^4 respectively. In (b) the inset shows the SAXS intensity scattered by a pure SDS solution in water ($S = 20$ mg.g^{-1}); the upturn of the intensity at low q values signals the emergence of attractive interactions.

3.4 Dynamical state diagram

In figure 8, we present the dynamical state diagram established from the results discussed in the previous sections, which specifies the state of the composites when both the polymer and surfactant concentrations are varied. The diagram exhibits a reentrant viscoelastic region and three solid regions delineated by four lines associated to the glass transition, the jamming transition, the saturation of the microgels by surfactant molecules, and the reentrant transition. The glass line is given by the divergence of the low-shear viscosity at $S_G = 18$ mg.g^{-1} (figure 4). The jamming line is obtained from the concentration dependence of the plateau modulus of the nanocomposites (figure 5): $S = S_J$ with $S_J = 24$ mg.g^{-1}. The saturation line is defined from the concentrations S_m above which microgels no longer adsorb surfactant molecules. We take

for S_m the surfactant concentration for which the plateau modulus G_0 is maximum (figure 5). The saturation line is well represented by the equation: $S_m = 1.63C$, which gives the adsorption capacity of the microgels. Finally, the reentrant line is where the nanocomposites experience a solid-to-liquid transition upon addition of surfactants (section 3.2.1).

At low surfactant concentrations, typically below $C_m \cong 18\ \text{mg.g}^{-1}$, microgels are swollen but their volume fraction remain smaller than the glass transition volume fraction. The number density of microgels is too small to allow the volume fraction to cross the glass transition line, even at maximum swelling. In addition, attractive interactions come into play at high surfactant concentrations causing a decrease of the viscosity (figure 4). The nanocomposites are viscoelastic liquids over the entire range of surfactant concentrations. For $C \geq C_m$, dynamical arrest takes place at the surfactant concentration S_G where the volume fraction becomes equal to the glass transition volume fraction. The value of the concentration C_m can be estimated from the expression $C = \phi\varphi\rho_P / Q$ which relates the microgel concentration to the effective volume fraction ϕ; φ is the volume fraction of polymer inside the particles in the collapsed state, ρ_P is the density of the polymer, and Q is the volume swelling ratio. Using the values of φ and ρ_P, which are known from a previous study on similar microgels [45] ($\varphi \cong 0.6$ and $\rho_P = 1.24\ \text{g.cm}^{-3}$) and $Q = 26$ at maximum swelling (Section 3.1), we estimate that $C_m \cong 17\ \text{mg.g}^{-1}$ at the glass transition ($\phi = 0.58$), which is in good agreement with the experimental value (18 mg.g^{-1}).

Above the glass transition line the volume fraction keeps on increasing as surfactant molecules continue to be added to the composites. For $S \cong 24\ \text{mg.g}^{-1}$, the jamming transition line is crossed and the composites solidify into a jammed glass termed jammed solid I in figure 8, which extends up to the saturation line. In this domain, the microgels interact through repulsive interactions originating from elastic contacts. This justifies that the rheological data shown in figures 5 and 6 match predictions for model soft elastic spheres [52,61,64]. Above the saturation line, attractive interactions force the microgels to associate and cause phase separation. In the regime termed jammed solid II, phase separation is arrested by the crowding which reduces the local mobility of the microgels. Attractive interactions are responsible for

significant deviations of the flow curves from the behaviour expected in the purely repulsive case (see figure 6).

At higher surfactant concentration, the attractive interactions ultimately provoke the melting of the glass at the reentrant solid-liquid transition. Liquid-like behaviour with a fully established terminal behaviour at low frequencies is attained at high surfactant concentrations above the reentrant solid-liquid transition (figures 2 (e)(f). The microstructure of the composites in the reentrant liquid phase resembles that of the solid composites above the saturation line with large scale heterogeneities typical of phase separation (figure 7).

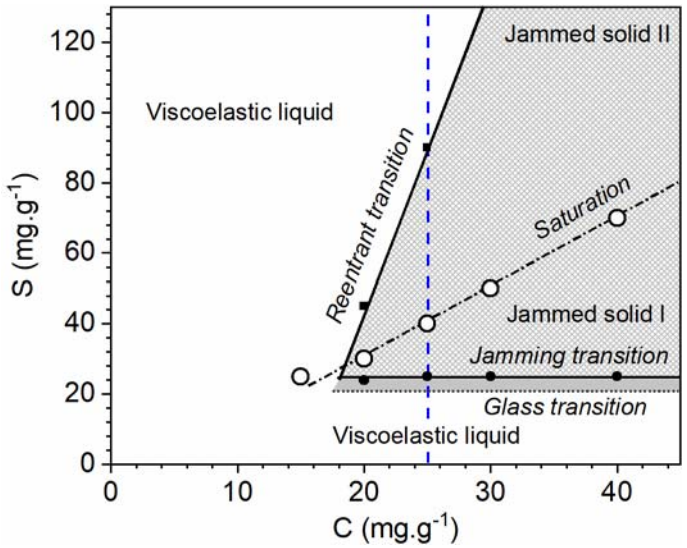

Figure 8. Dynamical state diagram giving the state of the composites and the transition lines as functions of the polymer and surfactant concentrations. The data reported in Figures 2, 3, and 7 refer to nanocomposites along the blue dashed line (C = 25 mg.g^{-1}).

4. Conclusion

Linear and non-linear rheology are powerful tools to fingerprint the rheological states of microgel-surfactant composites. Both techniques agree while providing complementary information. They give evidence for a wealth of possible states as the microgel and surfactant concentrations are increased: viscoelastic liquids, repulsive soft glasses, attractive soft glasses, weak gels, and reentrant viscoelastic liquids. Careful characterizations of the microstructures of these different composites by SAXS experiments and cryo-TEM observations reveal the importance of the interplay between enthalpic and entropic effects.

The primary role of the surfactant is to adsorb onto the polymeric network of the microgels and provoke their swelling. In a related study, we have shown that swelling is due to two effects: the variation of solvent quality (enthalpic effect) inside the microgels when the hydrophobic tail of the surfactant adsorbs onto the polymer thereby forming mixed polymer-surfactant micelles, and the osmotic pressure of the sodium counterions brought by the surfactant (entropic effect) [47]. Further studies will be useful to disentangle these two contributions. Interestingly, the volume fraction of the swollen microgels below saturation is entirely determined by the surfactant concentration independently of the microgel content. This means that, in this regime, there is no concentration-induced deswelling as it has been quantified and modelled in ionized polyelectrolyte microgel suspensions [45,46,65]. However, if the actual microgel volume fraction reaches a value close to 1 in dense packings, steric deswelling is also expected to occur [46].

Above the saturation concentration, the excess surfactant molecules self-assemble into micelles confined outside the microgels. The micelles act as depletants for the microgels and/or bridge neighbouring microgels, which results into attractive interactions and likely osmotic deswelling. These attractive interactions are responsible for the transformation of the repulsive jammed glasses into an arrested-phase-separated fluid and a viscoelastic reentrant liquid. Depletion forces and osmotic deswelling are at the origin of a wealth of phenomena in multicomponent mixtures of star polymers or microgels with linear polymers or hard spheres. Depletion interactions are responsible for the melting of hard sphere, microgel and star glasses upon addition of linear polymer [11,14,16,19,20]; the mixtures resolidify at high depletant concentration into an attractive glass and a gel, respectively. Similarly, hard sphere-like depletants have the capacity to transform star glasses into ergodic liquids, which then transforms into an arrested phase-separated solid [27,28]. The scenario discussed here for the case of adsorbing surfactant mixtures represents a different class of problem. Indeed, the melting of the jammed phase occurs through a progressive phase-separation mechanism, separation being first arrested by the jammed nature of the nanocomposites. The micelles

confined between the microgels push the microgels against one another, distort their environment, and progressively disrupt the elastic contacts at the origin of elasticity.

In conclusion our findings strongly emphasize the role of depletion and osmotic effects in tuning the microstructure and the rheology of soft colloidal mixtures. Adsorbing mixtures addressed here share some common rules with non-adsorbing situations but the overall picture is different. It will be interesting to use the results of our analysis to other guest-hosts situations where small moieties like proteins, nanoparticles, or oligomers are added to soft microgels.

Acknowledgments

S.G and M. C. gratefully acknowledge financial support from Coatex and ANRT under grant 2016/0988. S. G. and M. C. thank François Tournilhac, Jakob Langenbach, Dimitris Vlassopoulos and Javier Perez for help in the SAXS experiments, Dimitris Vlassopoulos for enlightening exchanges about osmotic effects in soft colloidal mixtures, and Clémentine Locatelli-Champagne and Benoit Magny for useful suggestions and discussions.

[1] Amin S and Palazzo G 2020 *Curr. Opin. Colloid Interface Sci.* **48** A1

[2] Loh X J 2016 *Polymers for personal care products and cosmetics* (Royal Society of Chemistry, Cambridge)

[3] Mezzenga R, Schurtenberger P, Burbidge A and Michel M 2005 *Nat. Mat.***4** 729

[4] Heilen W 2014 *Additives for Waterborne Coatings* (Vincentz Network, Hannover)

[5] Napper D H 1983 *Polymeric Stabilisation of Colloidal Dispersions* (Academic Press, London)

[6] Everett D H 1988 *Basic Principles of Colloid Science* (Royal Society of Chemistry, London)

[7] Asakura S and Oosawa F 1954 *J. Chem. Phys*. **22** 1255

[8] Vlassopoulos D and Cloitre M 2014 *Curr. Opin. Colloid Interface Sci*. **19** 561

[9] Vlassopoulos D and Cloitre M 2021 *Suspensions of soft colloids* in Theory and applications of colloidal suspension rheology ed Mewis J and Wagner N J (Cambridge University Press, New-York)

[10] Poon WCK 2002 *J. Phys.: Condens. Matter* **14** R859

[11] Pham K N, Puertas A M, Bergenholtz J, Egelhaaf S U, Moussaïd A, Pusey P N, Schofield A B, Cates M E, Fuchs M and Poon W C K 2002 *Science* **296** 104

[12] Zaccarelli E 2007 *J. Phys.: Condens. Matter* **19** 323101

[13] Lu P J, Zaccarelli E, Ciulla F, Schofield A B, Sciortino and Weitz D A 2008 *Nature* **453** 499

[14] Sciortino F 2002 *Nat. Mater*. **1** 145

[15] Tuinier R, Rieger J, and de Kruif C G 2003 *Adv. Colloid Interface Sci*. **103** 1

[16] Pham K N, Egelhaaf S U, Pusey P N and Poon W C K 2004 *Phys. Rev E* **69**,011503

[17] Pham K N, Petekidis G, Vlassopoulos D, Egelhaaf S U, Poon W C K and Pusey P N 2007 *J. Rheol.* **52** 649

[18] Sieglaff C L 1959 *J. Polym. Sci*. **12** 319

[19] Eckert T and Bartsch E 2002 *Phys. Rev. Lett.* **89** 125701

[20] Stiakakis E, Vlassopoulos D, Likos C N, Roovers J and Meier G 2002 *Phys. Rev. Lett.* **89** 208302

[21] Truzzolillo D, Vlassopoulos D, Munam A and Gauthier M 2014 *J. Rheol.* **58** 1441

[22] Wiemann M, Willenbacher N and Bartsch E 2012 *Colloids and Surfaces A: Physicochem. Eng. Aspects* **413** 78

[23] Eckert T and Bartsch E 2003 *Faraday Discuss* **123** 51

[24] Truzzolillo D, Vlassopoulos D and Gauthier M 2014 *Macromolecules* **44** 5043

[25] Burger S and Bartsch E 2014 *Colloids and Surfaces A: Physicochem. Eng. Aspects* **442** 6

[26] Mayer C, Zaccarelli E, Stiakakis E, Likos CN, Sciortino F, Munam A, Gauthier M, Hadjichristidis, Iatrou H, Tartaglia P, Löwen H and Vlassopoulos D 2008 *Nat. Mat.* **7** 780

[27] Marzi D, Capone B, Marakis J, Merola MC, Truzzolillo D, Cipelletti L, Moingeon F, Gauthier M, Likos C N, Vlassopoulos D and Camargo M 2015 *Soft Matter* **11** 8296

[28] Truzzolillo D, Marzi D, Marakis J, Capone B, Camargo M, Munam A, Moingeon F, Gauthier M, Likos C N and Vlassopoulos 2013 *Phys Rev Lett* **111** 208301

[29] Merola M G, Parisi D, Truzzolillo D and Vlassopoulos D 2018 *J. Rheol.* **62** 63

[30] Stiakakis E, Vlassopoulos D and Roovers J 2003 *Langmuir* **19** 6645

[31] Routh A F, Fernandez-Nieves A, Bradley M and Vincent B 2006 *J. Phys. Chem. B* **110** 12721

[32] Schneider M, Michels R, Pipich V, Goericgk G, Sauer V, Heim H-P and Hber K 2013 *Macromolecules* **46** 9091

[33] Schneider J, Werner M and Bartsch E 2018 *Soft Matter* **14** 3811

[34] Fussell S L, Bayliss K, Coops C, Matthews L, Li W, Briscoe W H, Faers M A, Royall C P and van Duijneveldt J S 2019 *Soft Matter* **15** 8578

[35] Bradley M, Bruno N and Vincent B 2005 *Langmuir* **21** 2750.

[36] Smith M H and Lyon L A 2011 *Macromolecules* **44** 8154

[37] Gao Y, Au-Yeung S C F and Wu C 1999 *Macromolecules* **32** 3674

[38] Barreiro-Iglesias R, Alvarez-Lorenzo C and Concheiro C A 2003 *Int. J. Pharm*. **258** 179

[39] Bradley M and Vincent B 2005 *Langmuir* **21** 8630

[40] Chari K, Hsu R, Bhargava P, Figura B, Yang W, Park J H, Clifford T and Kadir M 2013 *Langmuir* **29** 15521

[41] Li D, Hsu R, Figura B, Jacobs R, Li S, Horvath S, Clifford T and Chari K 2016 *Soft Matter* **12** 7150

[42] Kim J J, Park K 2001 *J. Control. Release* **77** 39

[43] Acciaro R, Gilanyi T, Varga I 2011 *Langmuir* **27** 7917

[44] Still T, Chen K, Alsayed A M, Aptowicz K B, Yodh A G 2013 *J. Colloid Interface Sci*. **405** 96

[45] Borrega R, Cloitre M, Betremieux I, Ernst B, and Leibler L 1999 *Europhys. Lett.* **47** 729

[46] Pellet C and Cloitre M 2016 *Soft Matter* **12** 3710

[47] Goujard S 2019 *Surfactant-activated microgels: structure and dynamics* (PhD Thesis, Paris Sciences et Lettres)

[48] Bird R B, Armstrong R C and Hassager O 1987 *Dynamics of polymeric liquids* (John Wiley & Sons, New York)

[49] http://www.synchrotron-soleil.fr/Recherche/LignesLumiere/SWING

[50] Cabane B and Duplessix R 1982 *J. Physique* **43**, 1529

[51] Schäfer K, Kolli H B, Christensen M K, Bore S L, Diezemann G, Gauss J, Milano G, Lund R and Cascella M 2020 *Angew. Chem*. **132** 18750

[52] Mohan L, Pellet C, Cloitre M and Bonnecaze R 2013 *J. Rheol.* **57** 1023

[53] Quemada D 1989 *Prog. Colloid Polymer Sci.* **79** 112

[54] Brady J F 1993 *J. Chem*. *Phys*. **99** 567

[55] Cheng Z, Zhu J, Chaikin P M, Phan S-E and Russel W B 2002 *Phys. Rev. E* **65** 041405

[56] Shewan H M, Stokes J 2015 *J. Colloid Interface Sci.* **442** 75

[57] Russel W B, Wagner N J and Mewis J 2013 *J. Rheol.* **57** 1555

[58] Scheffold F, Cardinaux F and Mason TG 2013 *J. Phys.: Condens. Matter* 25, 502101

[59] M van Hecke 2009 *J. Phys.: Condens. Matter* **22** 033101

[60] Cloitre M, Borrega R, Monti F and Leibler L 2003 *Phys. Rev. Lett.* 90 068303

[61] Liu T, Khabaz F, Bonnecaze R T and Cloitre M 2018 *Soft Matter* 14 7064

[62] Bonnecaze R T and Cloitre M 2010 *Adv. Polym. Sci*. **236** 117

[63] Jensen G V, Lund R, Gummel J, Narayanan T and Pedersen J S 2014 *Angew. Chem. Int. Ed*. **53**, 1

[64] Seth J, Mohan L, Locatelli-Champagne C, Cloitre M and Bonnecaze R T 2011 *Nat. Mat.* **10**, 838

[65] Fernández-Nieves A, Fernández-Barbero A, Vincent B, and de las Nieves F J 2003 *J. Chem. Phys.* **119**, 10383